Free Radical Research, January 2008; 42(1): 70–81

informa
healthcare

Thiols oxidation and covalent binding of BSA by cyclolignanic quinones are enhanced by the magnesium cation

ANTONIO E. ALEGRIA[1], PEDRO SANCHEZ-CRUZ[1], AJAY KUMAR[1], CARMELO GARCIA[1], FERNANDO A. GONZALEZ[2], AIMEE ORELLANO[2], BEATRIZ ZAYAS[3], & MARINA GORDALIZA[4]

[1]*Department of Chemistry, University of Puerto Rico–Humacao, Humacao, Puerto Rico,* [2]*Department of Chemistry, University of Puerto Rico–Rio Piedras, San Juan, Puerto Rico,* [3]*School of Environmental Affairs, Universidad Metropolitana, San Juan, Puerto Rico, and* [4]*Departamento de Química Farmacéutica, Campus Miguel de Unamuno, Facultad de Farmacia, Salamanca, Spain*

Accepted by Professor Jean Codet

(Received 5 June 2007; revised 2 November 2007)

Abstract

A novel cyclolignanic quinone, 7-acetyl-3′,4′-didemethoxy-3′,4′-dioxopodophyllotoxin (CLQ), inhibits topoisomerase II (TOPO II) activity. The extent of this inhibition was greater than that produced by the etoposide quinone (EQ) or etoposide. Glutathione (GSH) reduces EQ and CLQ to their corresponding semiquinones under anaerobic conditions. The latter were detected by EPR spectroscopy in the presence of $MgCl_2$ but not in its absence. Semiquinone EPR spectra change with quinone/GSH mol ratio, suggesting covalent binding of GSH to the quinones. Quinone-GSH covalent adducts were isolated and identified by ESI-MS. These orthoquinones also react with nucleophilic groups from BSA to bind covalently under anaerobic conditions. BSA thiol consumption and covalent binding by these quinones are enhanced by $MgCl_2$. Complex formation between the parent quinones and Mg^{+2} was also observed. Density functional calculations predict the observed blue-shifts in the absorption spectra peaks and large decreases in the partial negative charge of electrophilic carbons at the quinone ring when the quinones are complexed to Mg^{+2}. These observations suggest a possible role of Mg^{+2} chelation by these quinones in increasing TOPO II thiol and/or amino/imino reactivity with these orthoquinones.

Keywords: *Semiquinone, glutathione oxidation, Mg^{+2}, topoisomerase II, cyclolignanic quinine, glutathione adduct, BSA, BSA covalent binding*

Introduction

Three semi-synthetic derivatives of the cyclolignan podophyllotoxin, i.e. etoposide, teniposide and etopophos, are anticancer drugs widely used against several types of neoplasms including testicular and small-cell lung cancers, lymphoma, leukaemia, Kaposi's sarcoma and others [1,2]. Other podophyllotoxin derivatives have been synthesized such as those reported recently [3,4]. The activity of cyclolignans against several types of cancers has also been described [2,5,6]. Of these, etoposide is one of the most prescribed anticancer drugs in the world, being its primary molecular target topoisomerase II (TOPO II) [7]. The drug acts by stabilizing a covalent enzyme-cleaved DNA complex leading to the accumulation of permanent breaks in the genetic material which stimulates cell death pathways. Human TOPO II has been shown to be the molecular target for other

Correspondence: Antonio E. Alegria, Department of Chemistry, CUH Station, Humacao, P. R. 00791 USA. Tel: 787-852-3222. Fax: 787-850-9422. E-mail: ae_alegria@uprh.edu

ISSN 1071-5762 print/ISSN 1029-2470 online
DOI: 10.1080/10715760701790671

anti-tumour drugs as well (e.g. doxorubicin, mitoxantrone and mAMSA) [8]. One of the metabolic products of etoposide is the etoposide quinone (EQ). EQ was shown to be a powerful inhibitor of TOPO II [9]. EQ has been proposed to bind covalently both DNA and proteins [10]. In fact, several orthoquinone derivatives of EQ were found to be better TOPO II inhibitors than etoposide [11]. Thiol-reactive quinones and other thiol-reactive compounds such as *N*-ethylmaleimide (NEM), disulphiram and organic sulphides were shown to induce TOPO II-mediated DNA cleavage which suggests the possibility that cellular DNA damage could occur indirectly through thiolation of TOPO II [12,13]. Another TOPO II characteristic which is very relevant to the work presented here is that it requires magnesium ions for ATP binding and hydrolysis [14]. In addition, either magnesium or calcium ions are required for DNA cleavage [14]. In this work we show that a novel cyclolignanic quinone (CLQ) is a more potent TOPO II inhibitor than either etoposide or EQ. Applying the previous observation by Kalyanaraman et al. [15–17] and others [18,19] that orthosemiquinones can be stabilized by complexation to divalent metal cations, we also show that both of these orthoquinones are reduced to semiquinones by thiols in the presence of Mg^{+2} and that the semiquinone steady state concentrations increase, as well as thiol group concentrations in GSH and BSA decrease, in the presence of the magnesium cation. We also present spectroscopic evidence for GSH-quinone and GSH-semiquinone covalent adducts formation.

Materials and methods

Materials

The cyclolignanic quinone, 7-acetyl-3′,4′-didemethoxy-3′,4′-dioxopodophyllotoxin, CLQ (Figure 1), was synthesized as described previously [2]. Etoposide, $NaBH_4$, $NaIO_4$, GSH, *N*-ethylmaleimide (NEM), *o*-phthalaldehyde (OPA) and glutathione ethyl ester (GEE) were purchased from Sigma-Aldrich (St. Louis, MO). A stock solution of OPA was prepared by dissolving 50 mg of reagent grade OPA in 0.5 ml of methanol and diluting this to 5 mg/mL with 0.1 M sodium borate buffer at pH 9.90. A 10 mM stock solution of GSH and 1 mM GEE and were prepared daily. High purity (99.999%) magnesium chloride and NaCl were purchased from Aldrich. To measure Topoisomerase II activity we used a Topoisomerase II Drug Screening Kit (TopoGEN, Inc., Columbus, OH).

The etoposide quinone was synthesized as described elsewhere [20]. Briefly, etoposide was dissolved in dioxane/water and demethylated with sodium metaperiodate in the dark at 4°C. The resulting quinone was extracted with dichloromethane and crystallized twice by adding ether and stored in the dark at −20°C. The structure and purity of EQ were confirmed by TLC, ^{13}C NMR and IR spectroscopy: ^{13}C NMR (100 MHz, $CDCl_3$) ppm: 20.29 (1C;-CH_3), 38.04, 40.27, 45.24 (1C;-O-CH_3), 56.25, 66.52, 68.01 (1C;-CH_2), 68.34 (1C;-CH_2), 73.18, 74.47, 79.72, 99.87, 101.92, 102.03 (1C;-CH_2), 109.39, 110.17, 113.24, 123.78, 128.48, 129.27, 148.17, 149.31 (2C;-C = C-), 151.85, 157.43, 174.59 (1C;-C = O), 175.32 (1C;-C = O) and 178.23 (1C;-C = O). IR spectroscopy: carbonyl bands at 1768, 1693 and 1661 cm^{-1}.

Topoisomerase II relaxation activity assay

The enzyme relaxation activity of TOPO II was assessed with a TOPO II Drug Screening Kit (TopoGEN, Inc., Columbus, OH) using Human TOPO II (p170) (1 unit relaxes 0.5 μg of DNA in 30 min at 37°C) and 0.25 μg of DNA substrate (pRYG). Experimental drugs were dissolved in dimethylsulphoxide (DMSO) and were tested at a final concentration of 500, 250, 50, 25, 15 and 5 μM. Reactions (final volume 20 μl) were carried out for 30 min at 37°C, after which 2 μl of 10% sodium dodecylsulphate (SDS) was added. Bound protein was digested by incubation with proteinase K (final concentration 0.05 mg/ml) for 30 min at 37°C. Reactions were stopped by adding 5μl of electrophoresis loading buffer (0.25% bromophenol blue, 50% glycerol) and then were electrophoresed in a 1% agarose gel (150 V/120 min). To visualize the reaction products, the gel was stained with 0.5 μg/ml ethidium bromide for 45 min and destained for 30 min in distilled water. DNA bands were detected and quantitated in a Versa Doc imaging system (model 1000, Bio Rad).

Quinone reduction by GSH

A nitrogen saturated milimolar solution of either EQ or CLQ was prepared in DMSO. To this, deaereated solutions of GSH and cacodylate buffer (pH 7.4) or borate buffer (pH 9) were added. Quinone and GSH concentrations were optimized for best signal-to-noise ratio in the semiquinone EPR spectra in the presence or absence of 300 mM $MgCl_2$. Samples were also prepared in the presence of 900 mM NaCl. First derivative EPR spectra were acquired and analysed using an EMX X-band Bruker EPR spectrometer coupled to a computer. Well-resolved semiquinone first-derivative EPR spectra were simulated and optimized (best-fitted to the experimental spectra) using WINSIM [21], starting with hyperfine coupling available in the literature for EQ semiquinone, $EQ^{\bullet -}$ [15]. In many cases, a well-resolved spectrum was superimposed over a broad spectrum. The latter should correspond to aggregates of the semiquinone to neutral parent quinones and/or the corresponding hydroquinone. Similar aggregates in aqueous solutions have been observed for other semiquinones such

as anthracyclines [22]. A single broad line with peak-to-peak width of 2 Gauss with identical g-value to that of the aqueous phase species was used as the starting broad spectral component in the optimization process. Linewidths, hyperfine splittings, relative g-values, lineshapes and relative intensities were optimized in the composite spectra.

Sodium borohydride reduction of the quinone

A milimolar deaereated quinone solution in DMSO was mixed with a freshly prepared deareated aqueous $NaBH_4$ solution (at pH 11) in a 2:1 quinone-to-$NaBH_4$ molar ratio in the presence of $MgCl_2$ (final concentration of 300 mM in the sample). To this solution, an aliquot of cacodylic buffer was added to a final concentration of 50 mM in the sample (pH 7.4). A convenient amount of $NaIO_4$ was added to oxidize the hydroquinone to the semiquinone, if needed, to improve the EPR semiquinone signal-to-noise ratio.

Quinone–GSH covalent adduct characterization

The Michael addition products of EQ and CLQ by GSH, $SGEQH_2$ and $SGCLQH_2$ (Figure 1) were synthesized under exactly the same conditions as those used in samples where the glutathione-semiquinone adducts were detected (Figure 2). Thus, the syntheses were performed under anaerobic conditions, at pH 9 in borate buffer (25% DMSO v/v) and in the presence of 300 mM MgCl2, using a 1:2 quinone-to-GSH mol ratio. The reaction mixture was then cooled to precipitate as much as possible the $MgCl_2$ and decanted. The supernatant was chromatographed using a Biotage Flashmaster Personal on double C18 pre-packed Biotage Isolute Flash columns (150 ml each). A 20:80 methanol–water (v/v) mixture was used as eluent. Compounds thus obtained were lyophilized. White solid compounds were obtained. The following properties correspond to EQH_2SG and are consistent with data of this adduct reported previously [23]: M.P. 195°C, IR cm^{-1} (ATR Solid mode): 3293 (H-bond OH), 2924, 1766, 1532, 1502 and 1482. ^1H NMR (DMSO-*d6*) 400 MHz: δ 1.24 (3H, d), 1.94 (2H, m), 2.35 (2H, d), 2.84(1H, m), 3.07 (2H, t) 3.17 (4H, m), 3.36 (2H, m), 3.50 (3H, s), 3.57(8H, b), 3.65 (1H, s), 3.72 (2H, m), 4.09 (1H, t), 4.25 (3H, m), 4.50 (1H,dd), 4.73 (1H, d), 4.94 (1H, d), 5.39 (1H, d),

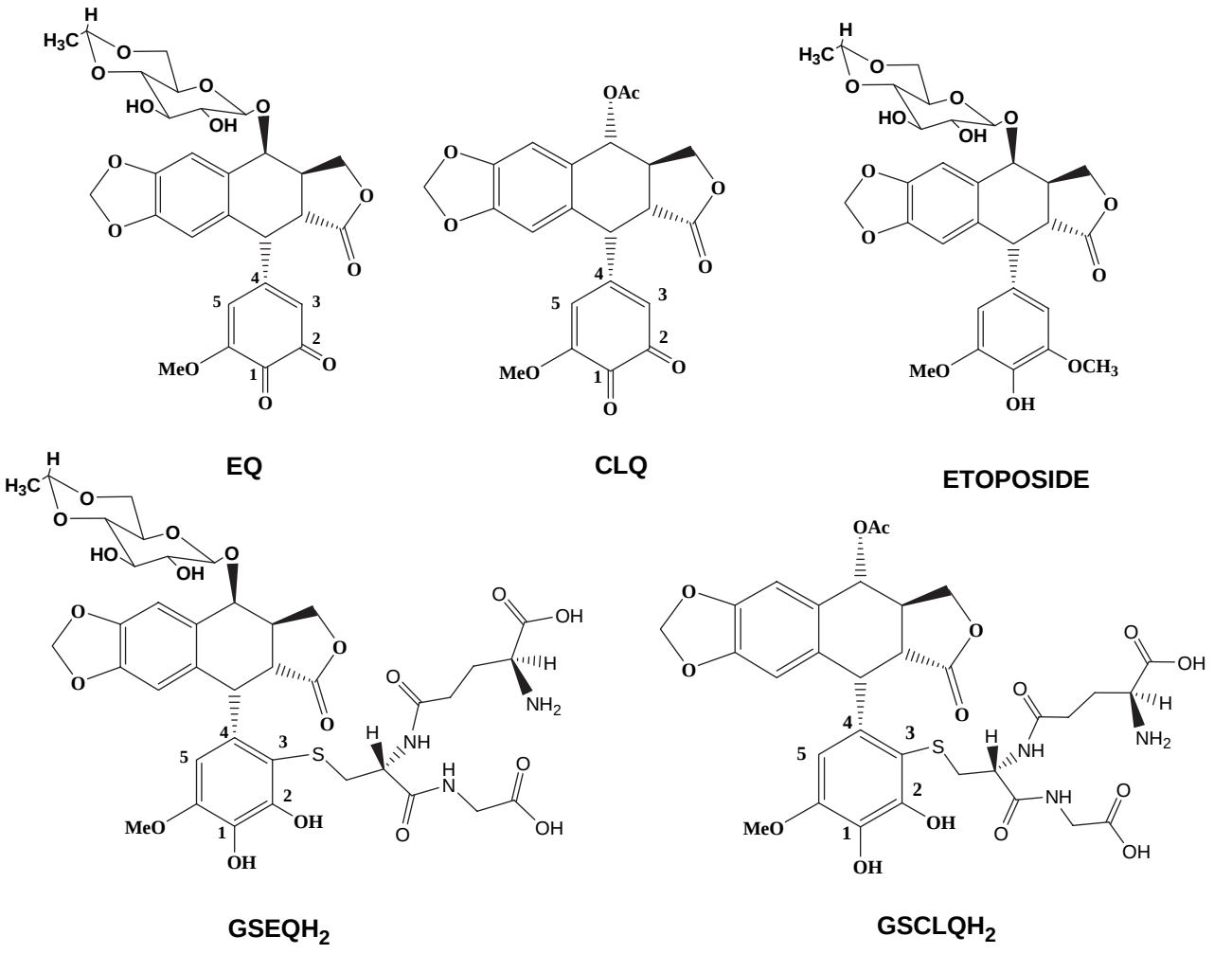

Figure 1. Compounds studied in this work.

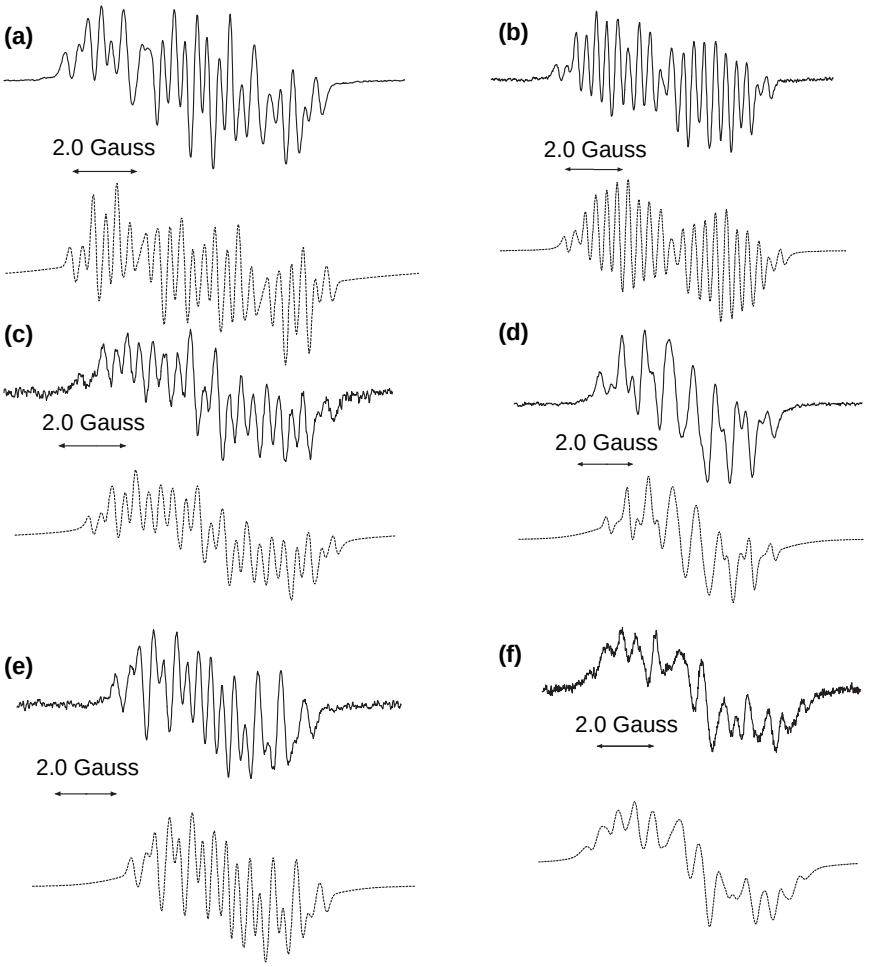

Figure 2. Epr spectra corresponding to the semiquinones EQ and CLQ after different reduction conditions under anaerobic conditions, at pH 9 in borate buffer (25% DMSO v/v) and in the presence of 300 mM $MgCl_2$. Spectra corresponds to $NaBH_4$ reduction of (A) CLQ and (B) EQ; (C) GSH reduction of EQ using a 6:1 EQ:GSH mol ratio; (D) GSH reduction of CLQ using a 1:2 CLQ:GSH mol ratio; (E) GSH reduction of EQ using a 1:2 EQ:GSH mol ratio and (F) GSH reduction using a 10:1 CLQ:GSH mol ratio. Dotted line spectra correspond to simulations and optimizations using WINSIM. With the exception of (F), two species are used: one corresponding to the resolved spectrum and another corresponding to a broad single line (starting with peak-to-peak width of $\sim$2.0 Gauss). The latter should be due to aggregates formation. In the case of (F), three species were needed to obtain best optimization: one corresponds to the broad spectral component, the other two are the GSH-free and the GSH-conjugated semiquinones in a 37:5 mol ratio, respectively. Hyperfine splittings are shown in Table I.

5.64 (1H, s), 6.02 (2H, dd), 6.31 (1H, s), 6.91 (1H, s) and 8.54 (2H, s). ^{13}C NMR (DMSO-*d6*) 100 MHz: δ 20.78, 27.17, 31.98, 37.15, 37.69, 38.55, 40.92, 41.56, 53.53, 53.79, 56.13, 56.20, 66.23, 66.82, 67.83, 73.11, 73.21, 74.89, 80.60, 99.05, 101.08, 101.76, 110.28, 116.02, 128.05, 133.52, 134.72, 146.20, 147.16, 148.29, 148.52, 171.16, 171.47, 172.39, 174.62 and 175.14.

ESI-MS analyses were performed on a Micromass Quattro Micro API triple quadrupole mass spectrometer with an ESI source (Micromass, Inc., Manchester, UK). Samples were injected into the MS by direct infusion through capillary tubing at a flow rate of 4 μL/min. The full scan ESI conditions for the monitored EQH_2SG adduct (MW = 879.8) were as follows: positive ionization mode, capillary voltage (0.90 kV), cone voltage (3.00 V), extractor voltage (1 V), source temperature (150°C), desolvation temperature (200°C) and desolvation gas flow of 400 L/h. The ESI conditions for the monitored $CLQH_2SG$ adduct (MW = 733.7) were as follows: positive ionization mode, capillary voltage (1.3 kV), cone voltage (4.00 V), extractor voltage (2.00 V), source temperature (100°C), desolvation temperature (200°C) and desolvation gas flow (400 L/h).

GSH consumption

Nitrogen-saturated mixtures containing 50 μM GSH, 50 mM cacodylic buffer at pH 7.4, with 300 mM $MgCl_2$ or 1 M NaCl and 50 μM EQ or CLQ and 25% by volume DMSO were incubated for 10 min. GSH was analysed by HPLC using fluorescence detection and pre-column derivatization with OPA following the method described by Cereser et al. [24]. This method is reported by the authors to be highly sensitive and precise for GSH determinations. All the procedures described here for GSH determinations

were performed under a N_2 atmosphere to avoid artifactual GSH oxidation by air at high pH. Reduced glutathione determination was performed by first mixing a 100 μL aliquot of the reacted mixture with 500 μL of 0.1 M sodium borate buffer (pH 9.90). From this, 300 μL were mixed with 100 μL of OPA solution and 5 μL of a GEE solution (used as internal standard) were also added. After 5 min at room temperature, the derivatized samples were neutralized by addition of 600 μL of 500 mM sodium phosphate at pH 7.00. This was followed by injection of a sample into the HPLC system.

After derivatization, samples were submitted to HPLC analysis using a μBondapack C_{18} (3.9×300 mM) column and eluted using an acetonitrile gradient in a 50 mM sodium acetate buffer, pH 6.20. The flow rate of elution was 0.7 mL/min. The column was washed daily with acetonitrile for 1 h and stored in 100% acetonitrile. The column was re-equilibrated to initial conditions for 60 min before injection. A Waters 1525 analytical HPLC system, equipped with a Waters 2475 multiwavelength fluorescence detector, was used, with excitation and emission wavelengths of 340 and 420 nm, respectively. GSH and GEE peak areas were measured and the GSH/GEE area ratios calculated. A standard curve was prepared using GSH/GEE peak area ratios for different GSH standard concentrations and used for the determination of GSH. All determinations here were repeated at least three times and the average of these determinations $\pm$ standard deviation is reported.

Covalent binding to BSA

Nitrogen-saturated mixtures containing 1.5 mM quinone, 1.5 mM BSA, 50 mM cacodylic buffer at pH 7.4 with 300 mM $MgCl_2$ or 900 mM NaCl and 25% by volume DMSO were incubated for 10 min. This was followed by Sephadex G-50 spun column filtration as described elsewhere [25,26]. Sephadex G-50 spun column filtration was repeated as many times as needed until an identical sample without BSA shows no quinone presence in the eluate. After this procedure, the protein was precipitated and washed with cold ethanol and redissolved in buffer as described by Deutscher [27]. The absorbance was read at a maximum wavelength in the 320–370 nm region for each quinone and corrected for the residual absorbance of GSH in this region using a BSA sample treated in the same manner as the QSD-containing BSA sample.

In order to detect the role of thiol groups in this binding process, NEM was used to block thiol groups in BSA. For this purpose, BSA was treated with a 100-fold molar excess of NEM for 1 h. Non-reacted NEM was then excluded from NEM-treated BSA also by Sephadex G-50 spun column filtration and ethanol precipitation and extraction. BSA concentration in the eluate was determined using BSA extinction coefficient (absorbance at 280 nm is 0.667 for 1 g BSA/ml) [28].

BSA thiol consumption

Samples submitted to the determination of BSA covalent binding described above were analysed for BSA thiol content after precipitation and redissolution. The protein thiol content assay described by Riener et al. [29] was used. In this assay, the absorbance of the 4-thiopyridone produced, after 4,4′-dithiodipyridine (DTDP) reduction by the protein thiols, is determined at 324 nm. Nitrogen-saturated BSA-containing samples were incubated with a 4-fold excess of DTDP in cacodylate buffer (pH 7.4) and the absorbance at 324 nm was monitored until a constant absorbance value was obtained (~60 min). The absorbance at 280 nm was also measured. To obtain the exclusive absorbance of BSA at 280 nm, the absorbance corresponding to 4-thiopyridone, bound quinone and DTDP was subtracted from the measured absorbance. Also the bound quinone absorbance at 324 nm was subtracted to obtain the corrected 4-thiopyridone absorbance. The ratio of the corrected absorbance at 324 nm to that corresponding to BSA at 280 nm was calculated. Thiol consumption percentage was determined after comparing these ratios with that of a BSA sample, of the same BSA batch, that was not reacted with quinones.

Binding of Mg^{+2} to quinones

The interaction of Mg^{+2} with quinines was monitored using an Agilent 8453 absorption spectrophotometer by observing changes in quinone spectra with addition of $MgCl_2$ at constant ionic strength in 50 mM cacodylate buffer (pH 7.4). Ionic strengths were levelled to that of a 1 M NaCl solution.

Density functional (DFT) calculations

Geometry pre-optimizations were performed *in vacuo* with the PM6 semi-empirical method using the Polak-Ribiere conjugated gradient protocol (1×10 convergence limit, 0.01–5 kcal/Å*mol RMS-limit) [30]. For all species, including the solvated Mg^{+2}, final optimizations were performed with DFT [B3LYP/6-31G(d) PTSCRF = (PCM, Solvent = Water)] using Gaussian 03 at the BobSCEd cluster (Earlham College Cluster Computing Group; Richmond, IN). All conformational and thermodynamic parameters were obtained with a DFT single point calculation. The energies involved in each of the following processes were obtained as the difference in the hartree energies for the following reactions in solution [ΔE (kcal/mol) = $(E_{prod} - E_{react})$*627.51]:

$$Q + Mg^{+2} \rightleftharpoons Q\text{-}Mg^{+2} \quad (1)$$

$$Q + e^{-} \longrightarrow Q^{\cdot -} \quad (2)$$

$$Q^{\cdot -} + Mg^{+2} \rightleftharpoons [Q\text{-}Mg]^{\cdot +} \quad (3)$$

The spectroscopic parameters were calculated with the ZINDO/s method.

Results and discussion

TOPO II inhibition

Figure 3 shows the inhibition of the DNA relaxation activity of TOPO II with the potency order etoposide $<$ EQ $<$ CLQ. EQ and other orthoquinone derivatives of etoposide have shown greater inhibition of this enzyme than etoposide [11].

GSH reduction of quinones

Anaerobic mixtures of GSH with either EQ or CLQ, only in the presence of Mg^{+2}, produce the corresponding EPR semiquinone spectra (Figure 2). It has been demonstrated previously that the orthosemiquinone stabilization by Mg^{+2} is due to a shift in the semiquinone disproportionation equilibrium towards the semiquinone [31]. Some broad component is observed in these EPR spectra indicating possible aggregation of a fraction of these semiquinones with neutral quinone or hydroquinone in analogy to what is observed for anthracycline semiquinones [22]. These observations are analogous to those previously made where complexation to multivalent cations is needed to stabilize *ortho*semiquinones while *para*semiquinones are not [31]. Anaerobic reduction of these quinones with $NaBH_4$ in the presence of $MgCl_2$ also produced the corresponding semiquinones (Figure 2). The presence of a spectral broad component is more pronounced when the spectrum is noisier (Figure 2). That is consistent with the presence of a larger concentration of EPR-silent species which should favour semiquinone aggregation with the latter, thus increasing the broad spectral component contribution to the total semiquinone area. Since the more noisy spectra were detected when GSH was used as reducing agent as compared to $NaBH_4$, the increase in the broad spectral component could also be produced by an increase in aggregation due to the presence of the glutathione substituent at the semiquinone. The hyperfine coupling constants of these semiquinones depend on the quinone/GSH mol ratio in the sample (Figure 2, Table I). A similar behaviour was observed for the reaction of 1,4-naphthoquinone with GSH [32]. In that case, the naphthosemiquinone EPR spectrum changed from that of the free semiquinone to the GSH-conjugated semiquinone with increase in the GSH/quinone mol ratio. In analogy, EPR spectra corresponding to larger quinone/GSH ratios are assigned to the free semiquinones $EQ^{\cdot -}$ and $CLQ^{\cdot -}$ and those corresponding to smaller quinone/GSH ratios assigned to GSH-conjugated semiquinones (Table I). GSH addition to the quinone ring has been detected in previous works for other orthoquinones [16] and EQ itself [23,33]. In fact, the GSH adduct of EQ has been recently found and characterized in myeloperoxidase-expressing human myeloid leukaemia HL60 cells when treated with etoposide for 30 min [23]. Evidence for the formation of the GSH adducts of EQ and CLQ, under the conditions stated above, is presented below. To our best knowledge, this is the first instance that EPR evidence have been presented to support the formation of GSH-$EQ^{\cdot -}$ and GSH-$CLQ^{\cdot -}$ species. A possible mechanism which explains the semiquinone-GSH adduct formation is discussed below.

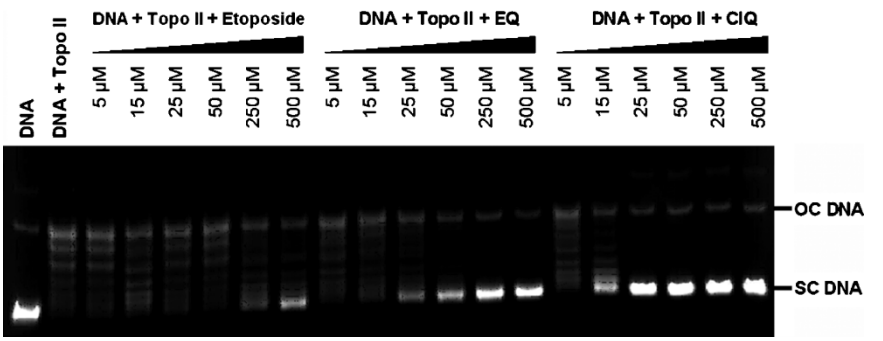

Figure 3. Inhibition of topoisomerase II activity. The DNA relaxation activity of topoisomerase II was determined as described in the Materials and methods section. The reactions were incubated at 37°C for 30 min in the presence of the indicated concentrations of etoposide (E), etoposide quinone (EQ) or CLQ. OC DNA stands for open circular DNA and SC DNA stands for supercoiled DNA. The experiment was repeated four times with similar results. A representative experiment is shown.

Table I. Semiquinone EPR hyperfine splitting constants after optimization of spectra in Figure 2.

Semiquinone and sample condition[a]	aH /Gauss
$[EQ\text{-}Mg]^{\bullet +}$ ($EQ+NaBH_4$)	0.73(3Hs), 0.35(1H), 3.41(1H), 0.66(1H), 0.83(1H)[b,c]
$[EQ\text{-}Mg]^{\bullet +}$ (6 EQ:1 GSH mol ratio)	0.74(3Hs), 0.36(1H), 3.39(1H), 0.63 (1H), 0.85 (1H)
$[EQ\text{-}Mg]^{\bullet +}$-GSH adduct (1 EQ:2 GSH mol ratio)	0.73(3Hs), 1.47(1H), 0.46(1H), 1.77(1H)
$[CLQ\text{-}Mg]^{\bullet +}$ ($NaBH_4+CLQ$)	0.67(3Hs), 0.37 (1H), 0.85(1H), 3.55(1H), 0.71(1H)
$[CLQ\text{-}Mg]^{\bullet +}$ (10 CLQ:1 GSH mol ratio)	0.54(3Hs), 0.35(1H), 3.41(1H), 1.17(1H), 0.71(1H)
$[CLQ\text{-}Mg]^{\bullet +}$-GSH adduct (1 CLQ:2 GSH mol ratio)	0.72(3Hs), 0.84(1H), 1.68(1H), 1.03(1H)

[a]in borate buffer, pH 9, and 25% DMSO v/v.
[b]values in parentheses correspond to the number of protons.
[c]similar to that reported previously in [15], i.e. 0.79(3Hs); 0.79(2Hs); 3.6(1H); 0.46(1H).

Quinone-glutathione adduct formation

The Michael addition products $SGEQH_2$ and $SGCLQH_2$ were identified as indicated in Materials and methods. ESI-MS results are shown in Figure 4. The spectrum presented in Figure 4A indicates the presence of a prominent signal at *m/z* 880.7 representing the protonated molecular ion $[M+H]^+$ of the $SGEQH_2$ of MW = 779.8. An increase of the

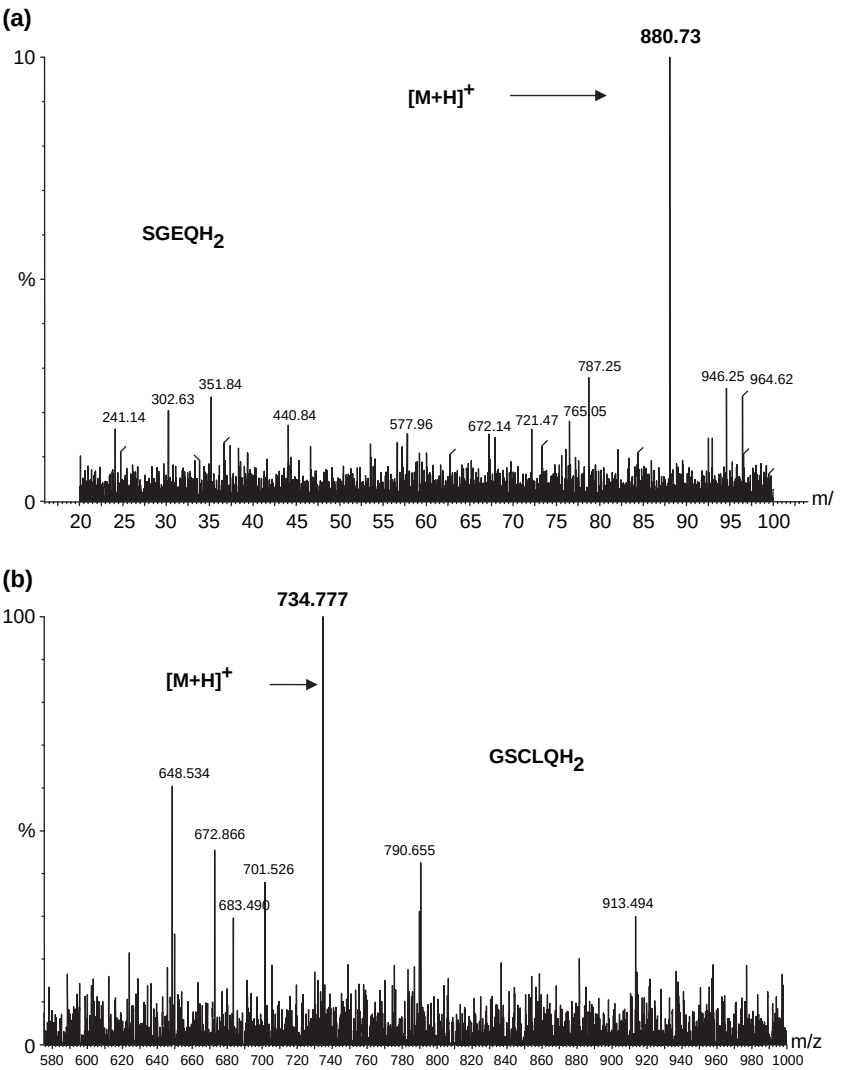

Figure 4. Full scan ESI-MS analyses of Michael addition products in mixtures of GSH with quinone: (A) $GSEQH_2$ (MW 879.8). The ESI-MS spectrum presents a prominent signal at *m/z* 880.73 amu representing the positive ion $[M+H]^+$ of the monitored adduct. Conditions for ESI analysis were: positive ionization mode, pump flow of 4 μL/min, capillary voltage of 0.90 kV, cone voltage of 3.00 V, extractor voltage of 1 V, source temperature of 150°C, desolvation temperature of 200°C and desolvation gas flow of 400 L/h. (B) $GSCLQH_2$ (MW 733.7). The ESI-MS spectrum presents a prominent signal at *m/z* 734.77 representing the positive ion $[M+H]^+$ of the monitored adduct. Conditions for ESI were: positive ionization mode, 4 μl flow rate, capillary voltage of 1.3 kV, cone voltage of 4.00 V, extractor voltage of 2.00 V, source temperature of 100°C, desolvation temperature of 200°C and desolvation gas flow of 400 L/h.

capillary voltage resulted in the formation of multiple fragments, decreasing the $[M+H]^+$ signal and increasing the signal intensity for the $[M+Na]^+$ ion (data not shown).

In relation to the formation of $SGCLQH_2$, the spectrum presented in Figure 4B clearly indicates the presence of a prominent signal at *m/z* 734.7 representing the protonated molecular ion $[M+H]^+$ of the $SGCLQH_2$ (MW = 733.7).

GSH consumption

Anaerobic mixtures containing GSH and either orthoquinone in the presence of Mg^{+2} show larger consumption of GSH relative to identical samples in the absence of Mg^{+2} (Figure 5). Samples containing Mg^{+2} but no quinone exhibited no GSH consumption, thus both Mg^{+2} and orthoquinone are needed for the GSH consumption enhancement. One of the GSH consuming reactions should be the GSH addition to the quinone ring [16,23,33]. Thus, not only the Mg^{+2} cation is stabilizing the orthosemiquinone species but also promoting GSH consumption.

BSA thiol consumption

Thiol consumption percentages in BSA after incubation, with or without quinone, in the presence or absence of $MgCl_2$, are shown in Figure 6. As shown in Figure 6, the percentages of consumed thiols in BSA after reacting with these quinones, in the presence of $MgCl_2$, are smaller than in the absence of this salt + quinone. Thus, as expected from the GSH consumption behaviour, the combination of $MgCl_2$ and orthoquinone induces larger BSA thiol consumption. In analogy to GSH consumption, it is expected that both BSA thiol oxidation and thiol addition to quinones should be accounted for the observed decrease in reduced thiol groups in BSA (see below).

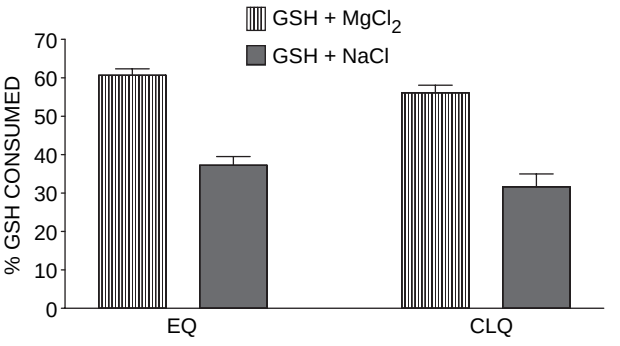

Figure 5. Percentage of GSH consumed after reacting for 10 min, under anaerobic conditions, 1.0 mM GSH with 50 μM quinone in cacodylate buffer (pH 7.4) in the presence or absence of 300 mM $MgCl_2$. The percentage of consumed GSH in the presence of $MgCl_2$ is calculated relative to a sample containing 300 mM $MgCl_2$ and no quinone. The percentage of consumed GSH in the presence of NaCl is calculated relative to a sample containing 900 mM NaCl and no quinone. The analysis was performed as described in the Materials and methods section.

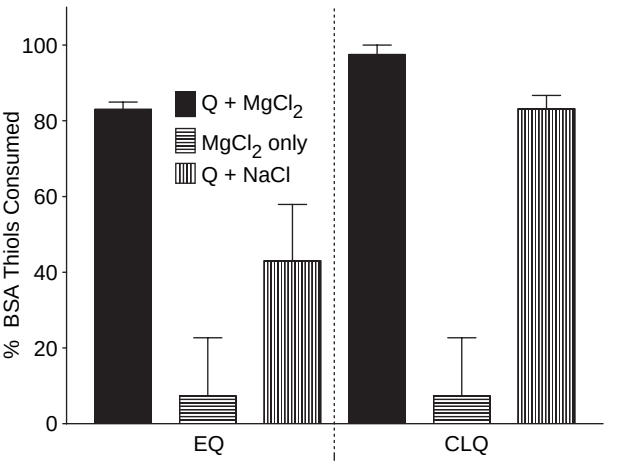

Figure 6. Percentage of thiol consumed after Sephadex G-50 spun filtration, BSA precipitation and redissolution of reacting mixtures (1.5 mM quinone + 1.5 mM BSA in 50 mM cacodylate, pH 7.4, anaerobic, in the presence or absence of 300 mM $MgCl_2$) determined by measuring the absorbance of the 4-thiopyridone produced, after 4,4′-dithiodipyridine (DTDP) reduction by protein thiols. These values are relative to a value of 0% consumption for samples containing 900 mM NaCl and in the absence of both $MgCl_2$ and quinone. NaCl was used to keep ionic strength constant.

BSA-quinone covalent adduct formation

After incubation of the quinones under study here with BSA under anaerobic conditions, followed by Sephadex spun-exclusion and protein precipitation and redissolution, absorption peaks of EQ and CLQ are still observed, indicating covalent binding of EQ and CLQ to BSA (Figure 7A). From the ratio of the quinone absorbance in the 320–380 nm region to that of BSA at 280 nm, the corresponding extinction coefficients and assuming that the quinone extinction coefficient is not changed upon binding BSA, the mol ratio of bound quinone to BSA was estimated (Figure 7B). NEM partially inhibits BSA binding of the quinones (more in the case of CLQ), thus binding could be due to quinone binding to amino or imino as well as to thiol groups in BSA. A similar behaviour was observed for the quinone avarone with BSA [34].

The interesting observation here is that, again, samples containing both *ortho*quinone and $MgCl_2$ produced larger amounts of quinone-BSA covalent adducts than those in the absence of $MgCl_2$.

Mg^{+2}-quinone complex

Addition of up to 300 mM $MgCl_2$ to solutions containing EQ or CLQ produces a shift of the

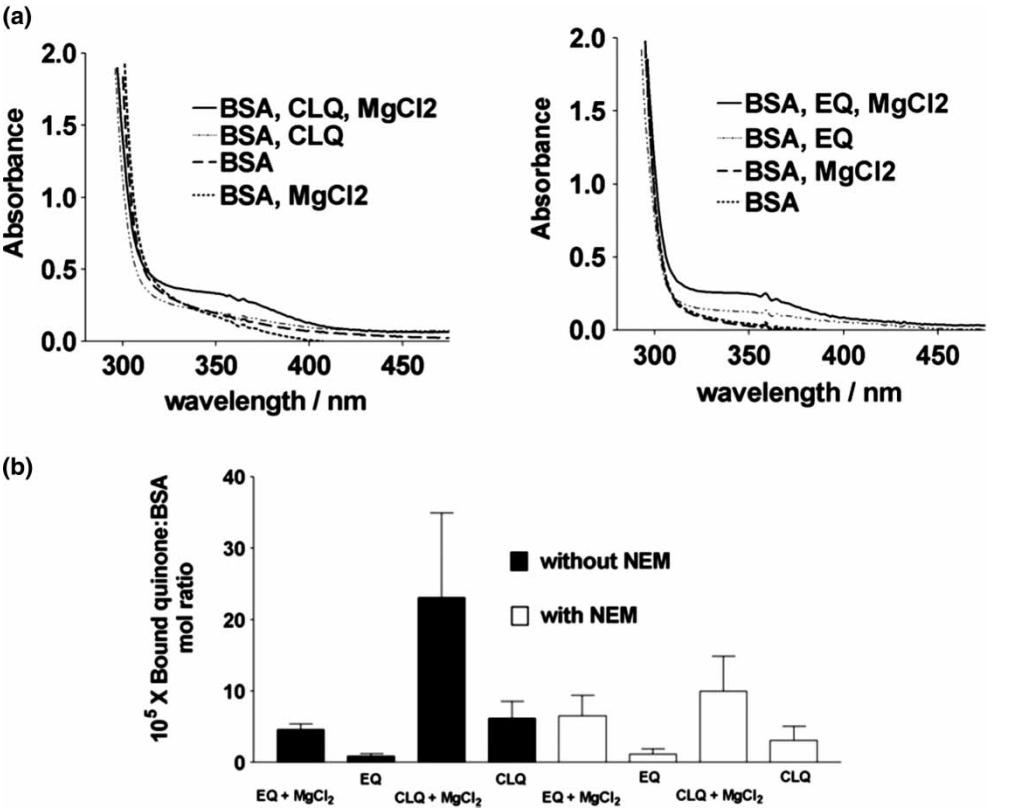

Figure 7. Covalent binding of quinones to BSA as detected from the absorption spectra (a) after Sephadex G-50 spun filtration and BSA precipitation and redissolution of mixing 1.5 mM quinone and 1.5 mM BSA in 50 mM cacodylate, pH 7.4, under anaerobic conditions, in the presence or absence of 300 mM $MgCl_2$. Quinones absorb near 350 nm. Estimated bound quinone to BSA mol ratios, obtained from the ratio of the bound quinone absorbance (peak maxima $\sim$350 nm) to that of BSA (at 280 nm), are shown in (b). The latter were calculated using the quinone extinction coefficients (extinction coefficients were determined as $(2.2 \pm 0.1) \times 10^3$ and $(3.3 \pm 0.2) \times 10^3$ M^{-1} cm^{-1} for EQ and CLQ, respectively, at 350 nm) and assuming these are not changed upon binding BSA. NaCl was used to keep an ionic strength identical to that corresponding to 900 mM NaCl. For samples containing NEM, BSA used was pretreated with a 100-fold excess of NEM, relative to BSA moles.

350 nm maxima in the absorption spectra of these quinones to $\sim$335 nm while increasing the extinction coefficients at the observed maxima (Figure 8). These features are not observed in the presence of 900 mM NaCl, indicating that a complex formation occurs between these orthoquinones and the Mg^{+2} cation. This complex formation should increase the redox potential of these orthoquinones, therefore stabilizing the formed semiquinone and promoting quinone alkylation by removing negative charge density from quinone ring carbons (see below).

Proposed semiquinone formation mechanism

Reports regarding Michael thiol addition to quinones are abundant in the literature [35–38] and its mechanism has been proposed since several years ago [39,40]. The proposed mechanism involves the

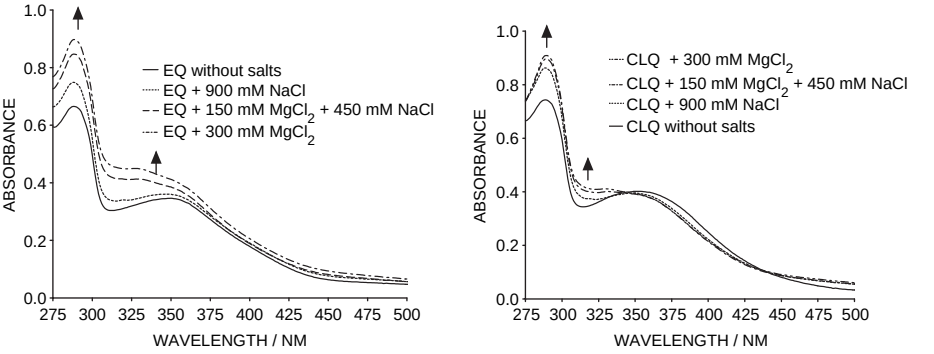

Figure 8. Effect of $MgCl_2$ addition in the absorption spectra of 150 μM EQ and 150 μM CLQ in 75:25 cacodylate buffer (50 mM, pH7.4):DMSO (v/v). Arrows show increase in absorbance maxima with an increase in $MgCl_2$ concentration.

$$Q + Mg^{+2} \rightleftharpoons Q{-}Mg^{+2} \quad (1)$$

$$Q{-}Mg^{+2} + GSH \rightleftharpoons GSQH_2 + Mg^{+2} \quad (4)$$

$$GSQH_2 + Q \rightleftharpoons GSQ^{\bullet -} + Q^{\bullet -} + 2H^{+} \quad (5)$$

$$GSQ^{\bullet -} + Mg^{+2} \rightleftharpoons [GSQ{-}Mg]^{\bullet +} \quad (6)$$

$$Q^{\bullet -} + Mg^{+2} \rightleftharpoons [Q{-}Mg]^{\bullet +} \quad (3)$$

$$Q{-}Mg^{+2} + [GSQ{-}Mg]^{\bullet +} \rightleftharpoons [Q{-}Mg]^{\bullet +} + GSQ{-}Mg^{+2} \quad (7)$$

Scheme 1. Proposed mechanism for the reactions stated in this work.

rate-limiting nucleophilic addition of the thiolate anion to the quinone (Q) to produce the corresponding thioether hydroquinone ($RSQH_2$). Thus, the corresponding semiquinone is produced after quinone + hydroquinone comproportionation (Scheme 1). The formation of oxidized GSH, GSSG, has been previously detected for the reaction of EQ with GSH, showing that GSH reduces this quinone to its semiquinone [33]. Thus, the possibility of direct reduction of the quinones to the semiquinones is also included in this Scheme. The Mg^{+2} ion is also included in Scheme 1 to show its role in promoting quinone alkylation and semiquinone stabilization. The magnesium-stabilized semiquinones $[GSQ\text{-}Mg]^{\bullet +}$ and $[Q\text{-}Mg]^{\bullet +}$ are the EPR-observed species. It is understandable from the proposed Scheme that the larger the GSH:quinone concentration ratio, the larger the probabilities of detecting a thiol-substituted semiquinone, as observed. Interestingly, at 10:1 CLQ-to-GSH mol ratio the unconjugated semiquinone, $[CLQ\text{-}Mg]^{\bullet +}$, was still detected in the presence of the GSH-conjugated semiquinone (Figure 2). However, at only a 6:1 EQ-to-GSH ratio the unconjugated semiquinone, $[EQ\text{-}Mg]^{\bullet +}$, was detected in the absence of the GSH-conjugated semiquinone. At first glance this could mean that $[GSCLQ\text{-}Mg]^{\bullet +}$ is more stable than $[GSEQ\text{-}Mg]^{\bullet +}$. However, the possibility of detecting a particular semiquinone should depend on the equilibrium position of reactions (3), (5), (6) and (7) of Scheme 1 and, thus, on the relative stabilities of neutral quinone and hydroquinone species.

Density functional (DFT) calculations

Our hypothesis for the Mg^{+2} enhancement of quinone substitution is that the Mg^{+2} ion is deshielding the substituted carbon of negative charge density, i.e. increasing the partial positive- or decreasing the partial negative charge of that carbon. This will facilitate the thiolate nucleophilic attack. Thus, we decided to calculate the corresponding partial charges of the quinone ring carbons. Figure 9 shows the optimized starting CLQ structure and those of the two possible Mg^{2+} complexes. In general, the conformation of the quinones, their complexes with

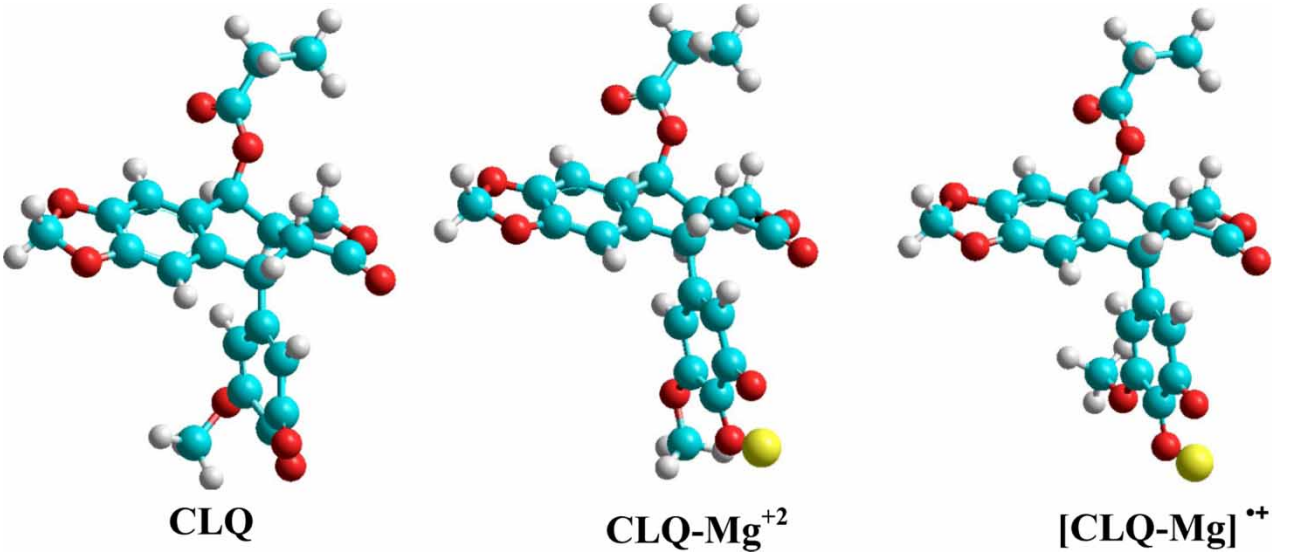

Figure 9. Starting CLQ structure and DFT-optimized structures of the corresponding complexes of CLQ and its semiquinone with Mg^{+2}.

Table II. Thermodynamic and spectroscopic parameters for the quinone and semiquinone species relevant to this work. Energies of each species were determined as the corresponding change in energy of reactions (1) to (3) in water.

Species	Energy (kcal/mol)	Partial atomic charge		λ^{a}_{max} (nm)
		C_3	C_5	
CLQ	–	−0.214	−0.278	373[0.17], 292[0.11]
CLQ-Mg^{+2}	22.8	−0.193	−0.235	344[0.23], 312[0.02], 285[0.11]
$CLQ^{\bullet}$ –	−81.1	−0.266	−0.317	254[0.09], 252[0.26]
$[CLQ\text{-}Mg]^{\bullet+}$	−121.9	−0.236	−0.267	329[0.14], 319[0.09], 250[0.46]
EQ	–	−0.218	−0.287	390[0.12], 300[0.04], 288[0.04], 254[0.05]
EQ-Mg^{+2}	8.1	−0.192	−0.266	306[0.32], 269[0.20]
$EQ^{\bullet}$ –	−81.6	−0.276	−0.313	308[0.03], 306[0.05], 263[0.18]
$[EQ\text{-}Mg]^{\bullet+}$	−180.2	−0.238	−0.279	332[0.10], 320[0.07], 252[0.42]

[a]Calculated absorption spectrum maximum wavelengths. Values in parentheses are the quantum oscillators. The latter are proportional to the predicted relative peak intensity.

Mg^{2+} and the corresponding reduced form do not change very much. The root mean square values of the differences in the atom coordinates for the quinone-benzene system are 0.07 for Q vs Q-Mg^{2+} and only 0.03 for Q-Mg^{2+} vs Q^{-}-Mg^{2+}. Nevertheless, the largest difference in conformation was observed for the C = O bond length and the torsion angle of the quinone-benzene system. For CLQ, for example, the C = O bond length increases from 1.23 Å to 1.34 Å for CLQ-Mg^{2+} and decreases to 1.29 Å for its reduced form. The torsion angle of the quinone-benzene ring changes accordingly. Measured relative to the central ring, their values are 126.2, 125.9 and 126.5° for CLQ, CLQ-Mg^{2+} and CLQ^{-}-Mg^{2+}, respectively.

Table II presents the DFT-theoretical values of the energy changes for reactions 1–3 and the atomic partial charges obtained for both of the electrophilic carbons at the quinone moiety. From the thermodynamics point of view, the formation of Q is an exothermic process. The corresponding electron affinities for CLQ and EQ are −81.1 and −81.6 kcal/mol, respectively. The complex formation of Q with Mg^{+2}, on the other hand, is not thermally favoured. For the corresponding semiquinone complexes, $[Q\text{-}Mg]^{\bullet+}$, energies go further down to –121.9 kcal/mol and −180.2 kcal/mol. The latter is in accordance with the observed semiquinone stabilization by Mg^{+2}. The smallest negative charges are located at the C_3 carbon of the $[Q\text{-}Mg]^{+2}$ complex, as compared to the same carbon position at $[Q\text{-}Mg]^{\bullet+}$ or the free quinone (Q). Thus, the nucleophilic attack of GS^{-} should occur preferentially at the C_3-atom of Q-Mg^{+2}, which has the smallest negative charge density in both quinone cases. The latter explains the enhancing effect of Mg^{+2} towards Michael addition of nucleophiles to these quinones.

The ZINDO/S predicted absorption properties of the Q-Mg^{+2} are in very good agreement with the experimental data. A blue-shift of the 360 nm band and the appearance of a new band at 320 nm are predicted for both quinones upon addition of $MgCl_2$.

In summary, the quinones EQ and CLQ are reduced to their corresponding semiquinones by GSH. The orthosemiquinones are detected in the presence of $MgCl_2$ but not in its absence, as reported previously for EQ. The salt $MgCl_2$ enhances GSH oxidation and BSA thiol consumption by EQ and CLQ. Furthermore, the covalent binding of these orthoquinones to BSA is mediated by both thiol groups and amino or imino groups and it is enhanced by this salt. Thus, not only the semiquinones of these orthoquinones are stabilized by interacting with Mg^{+2} but also the thiol oxidizing ability and binding to nucleophiles in BSA are also enhanced by the presence of the Mg^{+2} ion. These observations suggest a possible role of magnesium chelation by these quinones in TOPO II inhibition pathways of these compounds.

Acknowledgements

The authors are grateful for grants No. SO6-GM008216 and P20 RR-016470 from NIH (USA) for financial support of this work and the Earlham College Cluster Computing Group at Richmond, IN for sharing of computer time.

References

[1] Ayres DC, Loike JD. Lignans: Chemical, biological and clinical properties. Cambridge: Cambridge University Press; 1990.

[2] Gordaliza M, Castro MA, del Corral JM, Feliciano AS. Antitumor properties of podophyllotoxin and related compounds. Curr Pharm Design 2000;6:1811–1839.

[3] Wu Y, Zhang H, Zhao Y, Zhao J, Chen J, Li L. A new and efficient strategy for the synthesis of podophyllotoxin and its analogues. Org Lett 2007;9:1199–1202.

[4] Chen SW, Wang YH, Jin Y, Tian X, Zheng YT, Luo DQ, Tu YQ. Synthesis and anti-HIV-1 activities of novel podophyllotoxin derivatives. Bioorg Med Chem Lett 2007;17:2091–2095.

[5] Gordaliza M, Garcia PA, del Corral JM, Castro MA, Gomez-Zurita MA. Podophyllotoxin: distribution, sources, applications and new cytotoxic derivatives. Toxicon 2004;44:441–459.

[6] Botta B, Delle Monache G, Misiti D, Vitali A, Zappia G. Aryltetralin lignans: chemistry, pharmacology and biotransformations. Curr Med Chem 2001;8:1363–1381.
[7] Baldwin EL, Osheroff N. Etoposide, topoisomerase II and cancer. Curr Med Chem Anticancer Agents 2005;5:363–372.
[8] Liu LF. DNA topoisomerase poisons as antitumor drugs. Annu Rev Biochem 1989;58:351–375.
[9] Gantchev TG, Hunting DJ. The ortho-quinone metabolite of the anticancer drug etoposide (VP-16) is a potent inhibitor of the topoisomerase II/DNA cleavable complex. Mol Pharmacol 1998;53:422–428.
[10] Sinha BK, Myers CE. Irreversible binding of etoposide (VP-16-213) to deoxyribonucleic acid and proteins. Biochem Pharmacol 1984;33:3725–3728.
[11] Zhang YL, Shen YC, Wang ZQ, Chen HX, Guo X, Cheng YC, Lee KH. Antitumor agents, 130, Novel 4 beta-arylamino derivatives of 3′,4′-didemethoxy-3′,4′-dioxo-4-deoxypodophyllotoxin as potent inhibitors of human DNA topoisomerase II. J Nat Prod 1992;55:1100–1111.
[12] Wang H, Mao Y, Chen AY, Zhou N, LaVoie EJ, Liu LF. Stimulation of topoisomerase II-mediated DNA damage via a mechanism involving protein thiolation. Biochemistry 2001; 40:3316–3323.
[13] Lindsey RH Jr, Bromberg KD, Felix CA, Osheroff N. 1,4-Benzoquinone is a topoisomerase II poison. Biochemistry 2004;43:7563–7574.
[14] Marsh KL, Willmore E, Tinelli S, Cornarotti M, Meczes EL, Capranico G, Fisher LM, Austin CA. Amsacrine-promoted DNA cleavage site determinants for the two human DNA topoisomerase II isoforms alpha and beta. Biochem Pharmacol 1996;52:1675–1685.
[15] Kalyanaraman B, Premovic PI, Sealy RC. Characterization of free radicals produced during oxidation of etoposide (VP-16) and its catechol and quinone derivatives. An ESR study. Biochemistry 1989;28:4839–4846.
[16] Kalyanaraman B, Premovic PI, Sealy RC. Semiquinone anion radicals from addition of amino acids, peptides, and proteins to quinones derived from oxidation of catechols and catecholamines. An ESR spin stabilization study. J Biol Chem 1987; 262:11080–11087.
[17] Kalyanaraman B, Korytowski W, Pilas B, Sarna T, Land EJ, Truscott TG. Reaction between ortho-semiquinones and oxygen: pulse radiolysis, electron spin resonance, and oxygen uptake studies. Arch Biochem Biophys 1988;266:277–284.
[18] Sato A, Takagi K, Kano K, Kato N, Duine JA, Ikeda T. Ca^{2+} stabilizes the semiquinone radical of pyrroloquinoline quinine. Biochem J 2001;357:893–898.
[19] Lebedev AV, Ivanova MV, Ruuge EK. How do calcium ions induce free-radical oxidation of hydroxy-1,4-naphthoquinone? Ca^{2+} stabilizes the naphthosemiquinone anion-radical of echinochrome A. Arch Biochem Biophys 2003;413:191–198.
[20] Nemec J. 1986. US Pat. 4609644.
[21] Duling DR. Simulation of multiple isotropic spin-trap EPR spectra. J Mag Reson Ser B 1994;104:105–110.
[22] Schreiber J, Mottley C, Sinha BK, Kalyanaraman B, Mason RP. One-electron reduction of daunomycin, daunomycinone, and 7-deoxydaunomycinone by the xanthine/xanthine oxidase system: detection of semiquinone free radicals by electron spin resonance. J Am Chem Soc 1987;109:348–351.
[23] Fan Y, Schreiber EM, Giorgianni A, Yalowich JC, Day BW. Myeloperoxidase-catalyzed metabolism of etoposide to its quinone and glutathione adduct forms in HL60 cells. Chem Res Toxicol 2006;19:937–943.
[24] Cereser C, Guichard J, Drai J, Bannier E, Garcia I, Boget S, Parvaz P, Revol A. 'Quantitation of reduced and total glutathione at the femtomole level by high-performance liquid chromatography with fluorescence detection: application to red blood cells and cultured fibroblasts. J Chromatogr B Biomed Sci Appl 2001;752:123–132.
[25] Maniatis T, Fritsch EF, Sambrook J. Molecular cloning. A laboratory manual. New York: CSH Laboratory; 1985. p 466–467.
[26] Lusthof KJ, De Mol NJ, Janssen LH, Verboom W, Reinhoudt DN. DNA alkylation and formation of DNA interstrand cross-links by potential antitumour 2,5-bis(1-aziridinyl)-1,4-benzoquinones. Chem Biol Interact 1989;70:249–262.
[27] Deutscher MP. Maintaining protein stability. Methods Enzymol 1990;182:83–89.
[28] Stoscheck CM. Quantitation of protein. Methods Enzymol 1990;182:50–68.
[29] Riener CK, Kada G, Gruber HJ. Quick measurement of protein sulfhydryls with Ellman's reagent and with 4,4′-dithiodipyridine. Anal Bioanal Chem 2002;373:266–276.
[30] Jouyban A, Yousefi BH. A quantitative structure property relationship study of electrophoretic mobility of analytes in capillary zone electrophoresis. Comp Biol Chem 2003; 27:297–303.
[31] Alegria AE, Sanchez-Cruz P, Rivas L. Alkaline-earth cations enhance ortho-quinone-catalyzed ascorbate oxidation. Free Radic Biol Med 2004;37:1631–1639.
[32] Takahashi N, Schreiber J, Fischer V, Mason RP. Formation of glutathione-conjugated semiquinones by the reaction of quinones with glutathione: an ESR study. Arch Biochem Biophys 1987;252:41–48.
[33] Mans DR, Lafleur MV, Westmijze EJ, Horn IR, Bets D, Schuurhuis GJ, Lankelma J, Retel J. Reactions of glutathione with the catechol, the ortho-quinone and the semi-quinone free radical of etoposide. Consequences for DNA inactivation. Biochem Pharmacol 1992;43:1761–1768
[34] Belisario MA, Pecce R, Maturo M, De Rosa S. Arylation of sulfhydryl groups *in vitro* by the naturally occurring sesquiterpenoid benzoquinone avarone. Toxicology 1994;86:89–108.
[35] Wang X, Thomas B, Sachdeva R, Arterburn L, Frye L, Hatcher PG, Cornwell DG, Ma J. Mechanism of arylating quinone toxicity involving Michael adduct formation and induction of endoplasmic reticulum stress. Proc Natl Acad Sci USA 2006;103:3604–3609.
[36] Briggs MK, Desavis E, Mazzer PA, Sunoj RB, Hatcher SA, Hadad CM, Hatcher PG. A new approach to evaluating the extent of Michael adduct formation to PAH quinones: tetramethylammonium hydroxide (TMAH) thermochemolysis with GC/MS. Chem Res Toxicol 2003;16:1484–1492.
[37] Murty VS, Penning TM. Polycyclic aromatic hydrocarbon (PAH) ortho-quinone conjugate chemistry: kinetics of thiol addition to PAH ortho-quinones and structures of thioether adducts of naphthalene-1,2-dione. Chem Biol Interact 1992;84:169–188.
[38] Brunmark A, Cadenas E. Redox and addition chemistry of quinoid compounds and its biological implications. Free Radic Biol Med 1989;7:435–477.
[39] Wardman P. Bioreductive activation of quinones: redox properties and thiol reactivity. Free Radic Res Commun 1990;8:219–229.
[40] Wilson I, Wardman P, Lin TS, Sartorelli AC. Reactivity of thiols towards derivatives of 2- and 6-methyl-1,4-naphthoquinone bioreductive alkylating agents. Chem Biol Interact 1987;61:229–240.